Readout of Parafermionic States by Transport Measurements

Ida E. Nielsen,[1,2,*] Karsten Flensberg,[1] Reinhold Egger,[3] and Michele Burrello[1,2]
[1]Center for Quantum Devices, Niels Bohr Institute, University of Copenhagen, DK–2100 Copenhagen, Denmark
[2]Niels Bohr International Academy, University of Copenhagen, DK–2100 Copenhagen, Denmark
[3]Institut für Theoretische Physik, Heinrich Heine Universität, D-40225 Düsseldorf, Germany

(Received 13 September 2021; accepted 12 May 2022; published 13 July 2022)

Recent experiments have demonstrated the possibility of inducing superconducting pairing into counterpropagating fractional quantum Hall edge modes. This paves the way for the realization of localized parafermionic modes, non-Abelian anyons that share fractional charges in a nonlocal way. We show that, for a pair of isolated parafermions, this joint degree of freedom can be read by conductance measurements across standard metallic electrodes. We propose two complementary setups. We investigate first the transport through a grounded superconductor hosting two interacting parafermions. In the low-energy limit, its conductance peaks reveal their shared fractional charge yielding a three-state telegraph noise for weak quasiparticle poisoning. We then examine the two-terminal electron conductance of a blockaded fractional topological superconductor, which displays a characteristic $e/3$ periodicity of its zero-bias peaks in the deep topological regime, thus signaling the presence of parafermionic modes.

DOI: 10.1103/PhysRevLett.129.037703

Introduction.—The most common experimental signatures of the existence of Majorana zero-energy modes (MZM) [1] are based on charge transport measurements of hybrid superconductor-semiconductor devices [2–6]. These measurements can probe the existence of midgap excitations in topological superconductors, but do not provide a direct proof of their topological nature. Furthermore, transport does not allow for a readout of the fermionic parity shared by a pair of MZM: when coupling MZM to an external lead, electrons with energies below the superconducting (SC) gap tunnel into the system in a process that continuously flips the Majorana fermionic parity. This enables the detection of subgap states at the price of losing the information encoded in their parity, which is the main degree of freedom adopted in the proposals for topological quantum computation based on MZM. In this Letter, we show that this picture is fundamentally different when considering a fractionalized version of MZM, the so-called parafermionic zero-energy modes [7] (parafermions for short). We provide a model for the tunneling spectroscopy of two parafermionic SC devices and we show that transport measurements can be used to detect their shared degree of freedom.

Parafermions are localized topological excitations predicted to emerge in several heterostructures engineered by suitably coupling counterpropagating edge modes of fractional quantum Hall (FQH) states through an induced SC pairing [8–13]. This is a demanding objective since the strong magnetic fields required by FQH systems typically suppress the coherence of the necessary SC elements. Indeed, only very recently the combination of these two main ingredients has been experimentally achieved in a graphene-based Hall device contacted with a SC NbN electrode [14] (see also Ref. [15]). This system displayed evidence of crossed Andreev reflection of fractional quasiparticles, a key feature of parafermions hybridized with quantum Hall edge modes [16]. In the simplest case, based on the $\nu = 1/3$ Laughlin state, the resulting parafermionic topological superconductor is characterized by an emerging $\mathbb{Z}_6$ symmetry: a pair of parafermions causes a sixfold degeneracy of its ground states, which can be distinguished by their fractional charge $Q = qe/3$, with $q = 0, \ldots, 5$, such that Q is defined modulo the Cooper pair charge [8,9].

Building on the experimental setup of Ref. [14], we consider devices in which two parafermions are in contact with external electrodes (Fig. 1). The coupling between parafermions and metallic leads allows for electrons to tunnel in and out of the topological superconductor: the integer part of Q is therefore not conserved, but the fractional charge $\tilde{Q} = qe/3 \mod e$ is a conserved and topologically protected quantity, which can store quantum information and be read through transport measurements.

In the following, we present two complementary parafermion systems (see Fig. 1): First, we discuss a grounded device with interacting parafermions, whose energy splitting allows us to monitor their fractional charge $\tilde{Q}$ based on conductance measurements. Then, we examine a two-terminal blockaded setup with sizable charging energy; in the opposite limit of noninteracting parafermions, such system displays characteristic conductance signatures caused by these topological modes.

Modelling of the parafermions.—We begin our analysis by considering a SC device hosting two isolated parafermions. Such a device can be fabricated based on the

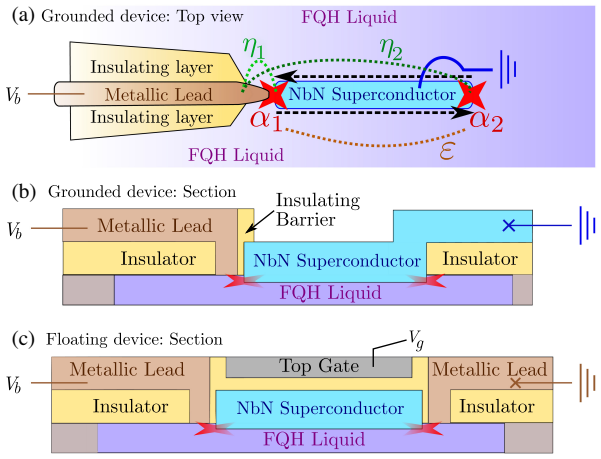

FIG. 1. Two-parafermion devices based on the SC pairing induced between chiral edge modes [dashed black arrows in (a)] by a NbN SC finger (light blue). (a) and (b) Top view and section of a grounded device. The NbN finger is in contact with the edges of a trench in a FQH liquid and defines two parafermions (red stars). A metallic lead (brown) is put in contact with the FQH liquid close to the left parafermion. The NbN finger is grounded through a SC bridge shown in (b). In (a) we schematically illustrate the tunnel couplings $\eta_{1,2}$ between lead and parafermions, and the parafermion overlap ε. (c) Coulomb blockaded device with a floating SC island. Its induced charge is controlled through the gate voltage V_g.

techniques adopted in Ref. [14]. A NbN SC thin finger is deposited in a trench etched in the bulk of a FQH liquid (Fig. 1). Two counterpropagating FQH edge modes appear on either side of the trench and are gapped by the proximity-induced superconductivity, allowed by the strong spin-orbit coupling of NbN. Differently from Refs. [14,16], we consider a device in which the superconductor is not coupled to any additional edge mode of the FQH liquid, such that the two resulting parafermions, α_1 and α_2, are isolated: given the bulk gap of the FQH liquid, they do not exchange fractional charges with the environment at low temperature.

The parafermionic operators α obey the following rules [9]:

$$\alpha_2\alpha_1 = e^{-i\pi/3}\alpha_1\alpha_2, \qquad \alpha_2^\dagger\alpha_1 = e^{i\pi/3}\alpha_1\alpha_2^\dagger, \tag{1}$$

with $\alpha_i^6 = \mathbb{1}$ and $\alpha_i^\dagger = \alpha_i^{-1}$. The zero-energy parafermions α_1 and α_2 induce a sixfold degeneracy of the ground states of this device which can be characterized by a suitable $\mathbb{Z}_6$ parity [17]: $e^{-i\pi/6}\alpha_2^\dagger\alpha_1 = e^{-i\pi q/3}$. Here q is a number operator with eigenvalues $0,\ldots,5$ counting fractional charges (mod 6) in the segment of the counterpropagating edge modes coupled with the superconductor and represents a joint observable of the two parafermions.

For energies below the induced SC gap, a weak coupling ε between α_1 and α_2 lifts the ground state degeneracy,

$$H_{\rm pf} = -\varepsilon e^{-i(\pi/6+\phi)}\alpha_2^\dagger\alpha_1 + \text{H.c.} = -2\varepsilon\cos(\pi q/3+\phi). \tag{2}$$

ε indicates the overlap of the two modes and $\phi \propto \mu L$ is a phase that depends on the chemical potential μ of the chiral edge modes and the SC finger length L [18,19].

The grounded N-SC device.—We couple this device with an external metallic lead [see Figs. 1(a) and 1(b)] and introduce the ladder operators l and $l^\dagger$ associated with electrons at the tunnel contact (the strong magnetic field polarizes the parafermions, therefore we consider only one spin species). The coupling between lead and parafermions causes both the coherent tunneling process of one electron moving into the superconductor, and the formation of a Cooper pair from an electron in the lead and an electron extracted from the FQH edges. The operators $\alpha_i^3 = (\alpha_i^\dagger)^3 \equiv \gamma_i$ anticommute and define two localized MZM. Therefore, in analogy with similar Majorana setups [20–24], we model the coupling as

$$H_c = i\sum_{j=1,2}\eta_j\gamma_j(e^{i\chi_j}l + e^{-i\chi_j}l^\dagger), \tag{3}$$

where $\eta_{1/2}e^{i\chi_{1/2}}$ is the tunneling amplitude between the lead and the left/right parafermion [Fig. 1(a)] with $\{\eta_j,\chi_j\}$ real and typically $\eta_1 \gg \eta_2$ (more general couplings and their renormalization group relevance are considered in the Supplemental Material [25]). H_c changes the charge Q by $\pm e$ and the Majorana operators γ_j allow us to rewrite $H_{\rm pf}$ by separating a fermionic and a fractional charge. The number q of fractional charges (modulo 6) can indeed be expressed in terms of the parity $p = i\gamma_2\gamma_1 = e^{i\pi q}$ and the fractional charge $e\tilde{q}/3 = eq/3 \bmod e$ (i.e., $\tilde{q} = 0, 1, 2$), such that each eigenstate $|q\rangle$ is recast in the form $|p,\tilde{q}\rangle$ (specifically, $e^{i\pi q/3} = pe^{i\pi 4\tilde{q}/3}$ [25]). The parafermion coupling becomes $H_{\rm pf} = -i2\varepsilon\gamma_2\gamma_1\cos(4\pi\tilde{q}/3+\phi)$, and is thus quadratic in the Majorana operators, while the charge $e\tilde{q}/3$ is a conserved quantity commuting with H_c.

As a result, the conductance of the two-terminal device in Figs. 1(a) and 1(b), between the normal lead and the grounded SC electrode, is derived through the corresponding two-Majorana setup [22] and is estimated by applying the Weidenmüller formula [37] for each value of the conserved fractional charge $e\tilde{q}/3$ separately [25]. In the low-energy approximation defined by $H = H_{\rm pf} + H_c$, valid when the SC gap and the lead bandwidth are the largest energy scales, the zero-temperature conductance reads

$$G_{\tilde{q}} = \frac{\frac{2e^2}{h}E^2(\eta_1^4+\eta_2^4+2\eta_1^2\eta_2^2\cos 2\tilde{\chi})}{\left(\frac{E^2-\Delta_\varepsilon^2(\tilde{q})-(\pi\nu_l\eta_1\eta_2\sin\tilde{\chi})^2}{\pi\nu_l}\right)^2 + E^2(\eta_1^2+\eta_2^2)^2}. \tag{4}$$

Here ν_l is the lead density of states and $E = eV_b$ represents the bias voltage V_b. $\Delta_\varepsilon(\tilde{q}) = 4\varepsilon\cos(4\pi\tilde{q}/3+\phi)$ is the parafermion energy splitting and $\tilde{\chi} = \chi_2 - \chi_1$. When the lead is coupled to a single parafermion ($\eta_2 = 0$) and the

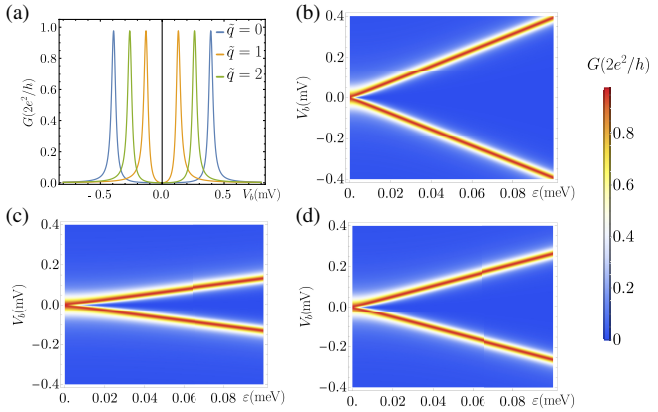

FIG. 2. Conductance of the grounded device as a function of V_b (a) and parafermion overlap ε (b),(c),(d) for $\nu_l = 1.727\ (\mathrm{meV})^{-1}$, $\eta_1 = 0.084$ meV, $\eta_2 = 0.0082$ meV, and $\tilde{\chi} = 0$. (a) Conductance peaks for $\varepsilon = 0.1$ meV. (b),(c),(d) System conductance vs ε for $\tilde{q} = 0$, 1, 2, respectively.

parafermions are not interacting ($\varepsilon = 0$), we observe a zero-bias peak for all values of $\tilde{q}$. For $\varepsilon \neq 0$ two conductance peaks appear at $E = \pm\Delta_\varepsilon(\tilde{q})$. Moreover, for $\tilde{\chi} = 0$ the peaks are quantized at $G = 2e^2/h$, analogously to two-Majorana devices [22,38].

This result can be generalized to finite temperature T [25]: In Fig. 2, choosing typical material parameters and $T = 20$ mK, we show results for the different fractional charges $e\tilde{q}/3$. We choose $\phi = 0.19$ for optimal splitting of the degeneracies in H_{pf}, and we emphasize that to read the degree of freedom $\tilde{q}$ from a conductance measurement, the parafermion coupling must be sufficiently large, $\varepsilon > T, \eta_1, \eta_2$, such that the different peaks are clearly resolved, as in Fig. 2(a).

If the two parafermions are not sufficiently isolated from other fractional modes, decoherence will affect $\tilde{q}$. Consider, for example, events in which the system is poisoned by fractional quasiparticles from the bulk or the external edges of the FQH liquid. If the poisoning rate is sizable compared with the current measurement time, the stationary state of the parafermion device becomes a statistical mixture of the three values of the parameter $\tilde{q}$, such that the transport readout displays all three peaks in Fig. 2(a) at the same time with suitable weights.

In this case, the resulting three-peak differential conductance would be hardly distinguishable from an analogous system hosting three nontopological subgap states, such as Andreev states which may form between the superconductor and the metallic lead. The observation of the conductance patterns in Fig. 2 is indeed not sufficient to establish the presence of parafermions. For weak poisoning, however, there is a crucial distinction between trivial bound states and parafermion systems. The former can be described by a simple scattering matrix approach and their transport is dictated by a single Landauer-Büttiker out-of-equilibrium steady state with a well-defined conductance. There is no possibility of changing their fractional charge for energies below the SC gap. An isolated two-parafermion system, instead, displays three different steady states labeled by $\tilde{q}$. If the poisoning rate is sufficiently weak compared to the current measurement time, the conductance at suitably chosen values of V_b will be affected by a three-state telegraph noise, similar to FQH interferometers [39,40]. The corresponding sudden jumps cannot be obtained without fractional subgap states and constitute a strong signature of the quasidegenerate parafermion states, without counterpart in Majorana devices.

The weak poisoning requirement may be hard to meet in experiments. Therefore, we next address complementary devices which, instead, display their main parafermion signatures at stronger poisoning rates and in the truly topological regime $\varepsilon \to 0$.

The Coulomb blockaded device.—For intermediate fractional quasiparticle poisoning, different signatures of the parafermions can be sought in the transport features of Coulomb blockaded SC islands. In the past years, several tunneling spectroscopy experiments have examined the onset of MZM through the two-terminal conductance of analogous devices [41–44]. Their topological phases can be distinguished by a different periodicity of the zero-bias conductance peaks as a function of the induced charge n_g [21,45,46]: $2e$ and $1e$ periodic patterns are observed in the trivial and topological phases, respectively.

In the following, we analyze the two-terminal conductance through a setup in which the NbN finger is floating and constitutes a SC island with strong charging energy. Its induced charge n_g can be varied by a top gate voltage V_g [Fig. 1(c)] and we consider two noninteracting metallic leads in proximity to the parafermions. The Hamiltonian of the floating SC island is modeled by

$$H_{\mathrm{SC}}(N_C, N_e, N', q, n_g) = H_{\mathrm{pf}}(q) + N_e\Delta_e + N'\Delta_{e/3} + E_C(2N_C + N_e + N'/3 + q/3 - n_g)^2. \quad (5)$$

Here we label the system states by the occupation numbers $|N_C, N_e, N', q\rangle$, where N_C refers to Cooper pairs in the SC island, N_e to quasielectron excitations in the device, N' to fractional quasiparticle excitations, and $eq/3$ is the charge of the localized parafermions as before. H_{SC} is determined by the following energy scales: the island charging energy E_C, the parafermion coupling ε, the energy gap of a quasielectron in the paired FQH edge modes Δ_e, and the energy gap for an $e/3$ quasiparticle excitation $\Delta_{e/3}$. To estimate ε, Δ_e, and $\Delta_{e/3}$, we model the system as a Luttinger liquid, describing the counterpropagating fractional edge modes beneath the SC finger [9]. Their proximity-induced SC pairing is treated at a mean-field level by introducing a crossed Andreev interaction Δ between the chiral modes [25], which is proportional to the SC gap of the NbN finger; it decays with its width [15] and decreases with magnetic field. The fractional

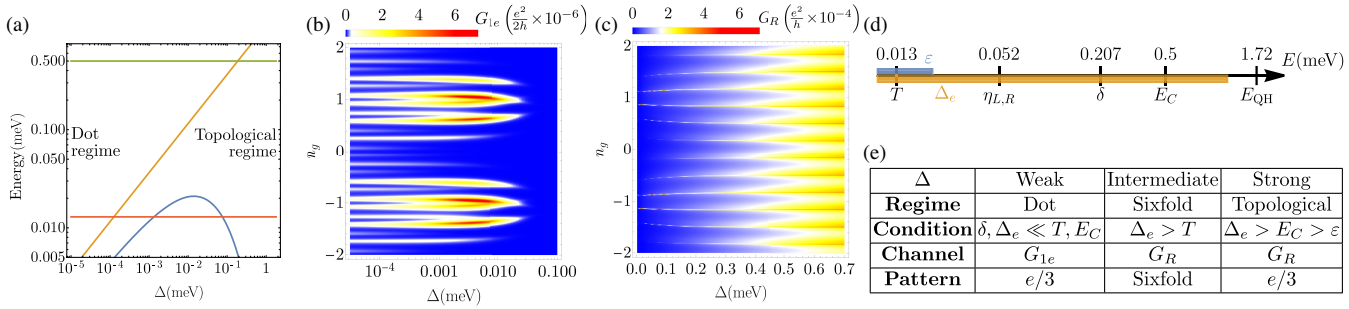

(e)

Δ	Weak	Intermediate	Strong
Regime	Dot	Sixfold	Topological
Condition	$\delta, \Delta_e \ll T, E_C$	$\Delta_e > T$	$\Delta_e > E_C > \varepsilon$
Channel	G_{1e}	G_R	G_R
Pattern	$e/3$	Sixfold	$e/3$

FIG. 3. Blockaded device coupled to two metallic leads with strengths $\eta_L = \eta_R = 0.052$ meV [25]. (a) Based on realistic parameters ($E_{\rm QH} = 1.72$ meV, $v = 10^5$ m/s, $L = 1$ μm), ε (blue) and Δ_e (orange) are compared with the charging energy $E_C = 0.5$ meV (green) and temperature $T = 0.15$ K (red). (b) Sequential tunneling zero-bias conductance G_{1e} as a function of Δ and n_g [from Eq. (7) and [25]]. (c) Resonant parafermion-mediated zero-bias conductance G_R [Eq. (7) and [25]]. This is typically the dominant contribution from moderate to large Δ. A sixfold pattern is observed for $\Delta \lesssim 0.3$ meV and evolves into an $e/3$-periodic pattern with increasing Δ. (d) Log scale summary of energies adopted in (b) and (c), including the dot energy level spacing δ. Ranges of ε and Δ_e are indicated by blue and orange. (e) Main properties of the discussed transport regimes.

quasiparticle gap is estimated through a semiclassical analysis: these quasiparticles can be described as solitons in a sine-Gordon model [18,25,47] and their mass results in $\Delta_{e/3} = \sqrt{8\Delta E_{\rm QH}/3\pi^3}$ as a function of Δ and the bulk gap $E_{\rm QH}$ of the FQH state with typical value $E_{\rm QH} \sim 2$ meV [25,48]. The results in Ref. [14] suggest a rough estimate $\Delta \lesssim 1$ meV. In the following, we adopt Δ as the main parameter to distinguish the system regimes and we exploit a simplified low-energy description. We approximate the behavior of both fractional and electron quasiparticles with noninteracting dynamics [25] and we minimize the quasielectron gap by $\Delta_e = 3\Delta_{e/3}$. Finally, the parafermion energy splitting ε is [18]

$$\varepsilon = \sqrt{\pi/2}\Delta_{e/3} \exp\left[-\sqrt{2\pi/3}(L\Delta_{e/3}/\hbar v)\right], \qquad (6)$$

where v the velocity of the chiral edge modes [see Fig. 3(a)].

Analogously to Majorana devices [42,46,49], transport across the system can be modeled by considering two main processes: (i) resonant tunneling of electrons mediated by parafermions, corresponding to electron teleportation mediated by the $\gamma_i = \alpha_i^3$ MZM [21], and (ii) single-electron incoherent sequential tunneling across gapped chiral states. A third process—sequential Andreev tunneling of Cooper pairs—is of less practical relevance and is discussed in the Supplemental Material [25].

Similarly to long grounded systems, the resonant tunnelling (i) accounts for transitions between q and $q+3$ mod 3 caused by the couplings of neighbouring lead and parafermion [analogous to Eq. (3) setting $\eta_2 = 0$ [25]]. Concerning the sequential tunneling (ii), we assume instead that electrons from the leads hop in and out of the island causing transitions between $N_e = 0$ and $N_e = 1$. We neglect scattering processes of the quasielectrons into fractional particles [25], such that N' is conserved. We phenomenologically capture the quasiparticle poisoning from the external environment by considering a thermal equilibrium distribution of the states $|N_C, N_e, N', q\rangle$ at temperature $T \ll E_C$. Hence, we estimate the total differential conductance by

$$\begin{aligned} G &= G_R + G_{1e} \\ &= \sum_{N_C,N_e,N',q} Z^{-1} e^{-H_{\rm SC}(N_C,N_e,N',q,n_g)/T} \\ &\quad \times \sum_{a=R,1e} \tilde{G}_a(n_g - [2N_C + N_e + (N'+q)/3]), \end{aligned} \qquad (7)$$

where the indices R and $1e$ represent resonant and sequential tunneling, respectively, and Z is the partition function. The conductances $\tilde{G}_a$ are estimated based on rate equations, analogously to the Majorana devices [46] (see the Supplemental Material [25] for details), and the resulting G_a are exemplified in Figs. 3(b) and 3(c).

For a realistic parameter choice, we can distinguish three main conductance patterns as a function of the SC pairing Δ, which we label as quantum dot, sixfold, and topological regimes [see table in Fig. 3(e)]. For $\Delta \to 0$, the gaps $\Delta_{e/3}, \Delta_e$, and ε vanish, thus the system behaves as a blockaded dot for fractional quasiparticles [50,51]. The electron sequential tunneling dominates and results in a complex set of zero-bias conductance peaks alternating with a $2e$ periodicity in the induced charge n_g. The location of these peaks depends on a further energy scale, $\delta = vh/2L$. In the example depicted in Fig. 3(b), the dot energy level spacing δ is comparable with E_C, thus yielding twelve irregular peaks in each $2e$ period for $\Delta \to 0$. Systems with $\delta, \Delta_e \ll E_C$, instead, would display an $e/3$ periodic pattern (not shown).

For intermediate pairing, the resonant tunneling becomes relevant and the most common zero-bias pattern displays only six dominant peaks repeating with $2e$ periodicity: We

call this regime *sixfold* [left side of Fig. 3(c), for $0.005\ \text{meV} \lesssim \Delta \lesssim 0.3\ \text{meV}$]. Such pattern emerges when Δ_e becomes larger than T.

Finally, for strong induced pairing ($\Delta \to E_{\text{QH}}$) in sufficiently long islands, the parafermion splitting drops, $\varepsilon \ll E_C < \Delta_e$ [Eq. (6) and Fig. 3(a)]. Therefore, the system is deeply in the topological regime and the zero-energy parafermions yield zero-bias G_R peaks repeating with a characteristic $e/3$ periodicity [Fig. 3(c), right side], analogously to the Majorana-mediated electron teleportation [21,46,52].

In conclusion, for typical experimental parameters ($L = 1\ \mu\text{m}$, $E_C = 0.5\ \text{meV}$), this $e/3$ periodicity signals the onset of the topological phase with strongly localized parafermions. Only for devices with negligible quasielectron excitation energy (dot regime with δ, $\Delta_e \ll T < E_C$), an additional $e/3$-periodic pattern may appear [table in Fig. 3(e)].

Conclusions.—We showed that parafermions in FQH setups with induced superconductivity [14] can be investigated through electronic transport measurements. In suitable two-terminal devices they give rise to conductance peaks analogously to MZM. In contrast with MZM, however, the ground states of isolated pairs of interacting parafermions can be distinguished through a current readout. The different values of their shared fractional charge yield different low-energy resonances in the conductance between a metallic electrode (tunnel coupled to the parafermions) and the SC background. This distinguishes our setup from devices characterized by the transport of fractional quasiparticles [53–59]. In the presence of weak quasiparticle poisoning we expect to observe a three-state telegraph noise, discriminating between parafermion and trivial electronic subgap states.

Complementary signatures of the parafermions are obtained from the analysis of blockaded devices. We studied the two-terminal conductance across a floating fractional superconductor as a function of its induced charge. For intermediate SC pairing and low temperature, the zero-bias conductance is characterized by a six-peak pattern repeating with $2e$ periodicity. The zero-bias peaks evolve towards an $e/3$-periodic pattern for strongly localized parafermions (similarly to fractional quasiparticle transport [54]).

The electronic tunneling spectroscopy we presented can be generalized to devices including additional leads or quantum dots, as recently proposed [60] for nontopological $\mathbb{Z}_4$ parafermions [61–63], and it can be integrated with additional fractional quasiparticle elements to develop novel topological quantum computation platforms based on parafermions.

We warmly thank Y. Gefen, F. Buccheri, A. C. C. Drachmann, M. Leijnse, M. Wauters, and A. B. Hellenes for useful discussions and K. Snizhko for helpful comments on a preliminary version of this manuscript and insightful observations. I. E. N. and M. B. are supported by the Villum foundation (research Grant No. 25310). We acknowledge support from the Deutsche Forschungsgemeinschaft (DFG) project Grant No. 277101999 within the CRC network TR 183 (subproject C01), as well as Germany's Excellence Strategy Cluster of Excellence Matter and Light for Quantum Computing (ML4Q) EXC 2004/1 390534769 and Normalverfahren Projektnummer EG 96-13/1. This project also received funding from the European Research Council (ERC) under the European Union's Horizon 2020 research and innovation program under Grant Agreement No. 856526, from the Danish National Research Foundation, and the Danish Council for Independent Research | Natural Sciences.

*Corresponding author.
ida.nielsen@nbi.ku.dk

[1] A. Y. Kitaev, Phys. Usp. **44**, 131 (2001).
[2] V. Mourik, K. Zuo, S. M. Frolov, S. R. Plissard, E. P. A. M. Bakkers, and L. P. Kouwenhoven, Science **336**, 1003 (2012).
[3] M. T. Deng, S. Vaitiekėnas, E. B. Hansen, J. Danon, M. Leijnse, K. Flensberg, J. Nygård, P. Krogstrup, and C. M. Marcus, Science **354**, 1557 (2016).
[4] F. Nichele, A. C. C. Drachmann, A. M. Whiticar, E. C. T. OFarrell, H. J. Suominen, A. Fornieri, T. Wang, G. C. Gardner, C. Thomas, A. T. Hatke, P. Krogstrup, M. J. Manfra, K. Flensberg, and C. M. Marcus, Phys. Rev. Lett. **119**, 136803 (2017).
[5] O. Gül, H. Zhang, J. D. S. Bommer, M. W. A. de Moor, D. Car, S. R. Plissard, E. P. A. M. Bakkers, A. Geresdi, K. Watanabe, T. Taniguchi, and L. P. Kouwenhoven, Nat. Nanotechnol. **13**, 192 (2018).
[6] M.-T. Deng, S. Vaitiekėnas, E. Prada, P. San-Jose, J. Nygård, P. Krogstrup, R. Aguado, and C. M. Marcus, Phys. Rev. B **98**, 085125 (2018).
[7] P. Fendley, J. Stat. Mech. (2012) P11020.
[8] N. H. Lindner, E. Berg, G. Refael, and A. Stern, Phys. Rev. X **2**, 041002 (2012).
[9] D. J. Clarke, J. Alicea, and K. Shtengel, Nat. Commun. **4**, 1348 (2013).
[10] A. Vaezi, Phys. Rev. B **87**, 035132 (2013).
[11] M. Cheng, Phys. Rev. B **86**, 195126 (2012).
[12] R. S. K. Mong, D. J. Clarke, J. Alicea, N. H. Lindner, P. Fendley, C. Nayak, Y. Oreg, A. Stern, E. Berg, K. Shtengel, and M. P. A. Fisher, Phys. Rev. X **4**, 011036 (2014).
[13] M. Barkeshli and X.-L. Qi, Phys. Rev. X **4**, 041035 (2014).
[14] Ö. Gül, Y. Ronen, S. Y. Lee, H. Shapourian, J. Zauberman, Y. H. Lee, K. Watanabe, T. Taniguchi, A. Vishwanath, A. Yacoby, and P. Kim, arXiv:2009.07836.
[15] G.-H. Lee, K.-F. Huang, D. K. Efetov, D. S. Wei, S. Hart, T. Taniguchi, K. Watanabe, A. Yacoby, and P. Kim, Nat. Phys. **13**, 693 (2017).
[16] D. J. Clarke, J. Alicea, and K. Shtengel, Nat. Phys. **10**, 877 (2014).
[17] M. Burrello, B. van Heck, and E. Cobanera, Phys. Rev. B **87**, 195422 (2013).
[18] C. Chen and F. J. Burnell, Phys. Rev. Lett. **116**, 106405 (2016).

[19] S. Groenendijk, A. Calzona, H. Tschirhart, E. G. Idrisov, and T. L. Schmidt, Phys. Rev. B **100**, 205424 (2019).
[20] J. Nilsson, A. R. Akhmerov, and C. W. J. Beenakker, Phys. Rev. Lett. **101**, 120403 (2008).
[21] L. Fu, Phys. Rev. Lett. **104**, 056402 (2010).
[22] K. Flensberg, Phys. Rev. B **82**, 180516(R) (2010).
[23] A. Zazunov, A. Levy Yeyati, and R. Egger, Phys. Rev. B **84**, 165440 (2011).
[24] L. Fidkowski, J. Alicea, N. H. Lindner, R. M. Lutchyn, and M. P. A. Fisher, Phys. Rev. B **85**, 245121 (2012).
[25] See Supplemental Material at http://link.aps.org/supplemental/10.1103/PhysRevLett.129.037703, which includes the Refs. [26–36].
[26] J. Danon, A. B. Hellenes, E. B. Hansen, L. Casparis, A. P. Higginbotham, and K. Flensberg, Phys. Rev. Lett. **124**, 036801 (2020).
[27] N. W. Ashcroft and N. D. Mermin, *Solid State Physics* (W. B. Saunders Company, Philadelphia, 1976), Chap. 2.
[28] E. Sela, Y. Oreg, S. Plugge, N. Hartman, S. Lüscher, and J. Folk, Phys. Rev. Lett. **123**, 147702 (2019).
[29] Y. Kasahara, T. Ohnishi, Y. Mizukami, O. Tanaka, Sixiao Ma, K. Sugii, N. Kurita, H. Tanaka, J. Nasu, Y. Motome, T. Shibauchi, and Y. Matsuda, Nature (London) **559**, 227 (2018).
[30] V. Crépel, B. Estienne, and N. Regnault, Phys. Rev. Lett. **123**, 126804 (2019).
[31] C. W. J. Beenakker, SciPost Phys. Lect. Notes **15** (2020).10.21468/SciPostPhysLectNotes.15
[32] K. Flensberg, F. von Open, and A. Stern, Nat. Rev. Mater. **6**, 944 (2021).
[33] D. Feinberg, Eur. Phys. J. B **36**, 419 (2003).
[34] J. Danon and K. Flensberg, Phys. Rev. B **91**, 165425 (2015).
[35] C. Reeg, J. Klinovaja, and Daniel Loss, Phys. Rev. B **96**, 081301(R) (2017).
[36] R. V. Mishmash, D. Aasen, A. P. Higginbotham, and J. Alicea, Phys. Rev. B **93**, 245404 (2016).
[37] I. Aleiner, P. Brouwer, and L. Glazman, Phys. Rep. **358**, 309 (2002).
[38] K. T. Law, Patrick A. Lee, and T. K. Ng, Phys. Rev. Lett. **103**, 237001 (2009).
[39] S. An, P. Jiang, H. Choi, W. Kang, S. H. Simon, L. N. Pfeiffer, K. W. West, and K. W. Baldwin, arXiv:1112.3400.
[40] B. Rosenow and S. H. Simon, Phys. Rev. B **85**, 201302(R) (2012).
[41] S. M. Albrecht, A. P. Higginbotham, M. Madsen, F. Kuemmeth, T. S. Jespersen, J. Nygård, P. Krogstrup, and C. M. Marcus, Nature **531**, 206 (2016).
[42] S. M. Albrecht, E. B. Hansen, A. P. Higginbotham, F. Kuemmeth, T. S. Jespersen, J. Nygård, P. Krogstrup, J. Danon, K. Flensberg, and C. M. Marcus, Phys. Rev. Lett. **118**, 137701 (2017).
[43] T. Kanne, M. Marnauza, D. Olsteins, D. J. Carrad, J. E. Sestoft, J. de Bruijckere, L. Zeng, E. Johnson, E. Olsson, K. Grove-Rasmussen, and J. Nygård, Nat. Nanotechnol. **16**, 776 (2021).
[44] S. Vaitiekėnas, G. W. Winkler, B. van Heck, T. Karzig, M.-T. Deng, K. Flensberg, L. I Glazman, C. Nayak, P. Krogstrup, R. M. Lutchyn, and C. M. Marcus, Science **367**, eaav3392 (2020).
[45] R. Hützen, A. Zazunov, B. Braunecker, A. Levy Yeyati, and R. Egger, Phys. Rev. Lett. **109**, 166403 (2012).
[46] B. van Heck, R. M. Lutchyn, and L. I. Glazman, Phys. Rev. B **93**, 235431 (2016).
[47] G. Mussardo, *Statistical Field Theory: An Introduction to Exactly Solved Models in Statistical Physics*, 2nd ed. (Oxford University Press, New York, 2020), Chap. 16.
[48] K. I. Bolotin, F. Ghahari, M. D. Shulman, H. L. Stormer, and P. Kim, Nature **462**, 196 (2009).
[49] E. B. Hansen, J. Danon, and K. Flensberg, Phys. Rev. B **97**, 041411(R) (2018).
[50] V. J. Goldman and B. Su, Science **267**, 1010 (1995).
[51] S. M. Mills, D. V. Averin, and X. Du, Phys. Rev. Lett. **125**, 227701 (2020).
[52] M. Thamm and B. Rosenow, Phys. Rev. Research **3**, 023221 (2021).
[53] M. Barkeshli, Y. Oreg, and X.-L. Qi, arXiv:1401.3750.
[54] Y. Kim, D. J. Clarke, and R. M. Lutchyn, Phys. Rev. B **96**, 041123(R) (2017).
[55] K. Snizhko, R. Egger, and Y. Gefen, Phys. Rev. B **97**, 081405(R) (2018).
[56] K. Snizhko, F. Buccheri, R. Egger, and Y. Gefen, Phys. Rev. B **97**, 235139 (2018).
[57] L. Mazza, J. Viti, M. Carrega, D. Rossini, and A. De Luca, Phys. Rev. B **98**, 075421 (2018).
[58] N. Schiller, E. Cornfeld, E. Berg, and Y. Oreg, Phys. Rev. Research **2**, 023296 (2020).
[59] A. E. Svetogorov, D. Loss, and J. Klinovaja, Phys. Rev. B **103**, L180505 (2021).
[60] R. L. R. C. Teixeira and L. G. G. V. Dias da Silva, Phys. Rev. Research **3**, 033014 (2021).
[61] L. Mazza, F. Iemini, M. Dalmonte, and C. Mora, Phys. Rev. B **98**, 201109(R) (2018).
[62] A. Calzona, T. Meng, M. Sassetti, and T. L. Schmidt, Phys. Rev. B **98**, 201110(R) (2018).
[63] A. Chew, D. F. Mross, and J. Alicea, Phys. Rev. B **98**, 085143 (2018).